MNRAS 000, 1–5 (2025) Preprint 30 August 2025 Compiled using MNRAS LATEX style file v3.3

Constrain star formation criteria by comparing statistics of SNe-driven bubbles in simulations with PHANGS observations.

Hao-Sheng Wang[1]★, Caleb R. Choban[2],
[1]Department of Astronomy, University of Virginia, Charlottesville, VA 22904, USA
[2]Department of Astronomy, Indiana University, Bloomington, IN 47405, USA

Accepted XXX. Received YYY; in original form ZZZ

ABSTRACT

Star formation and subsequent stellar feedback shape the interstellar medium (ISM) and regulate the evolution of galaxies. With the James Webb Space Telescope (JWST), mid-infrared imaging now resolves feedback-driven structures in nearby galaxies on ∼10 pc scales. In particular, polycyclic aromatic hydrocarbon (PAH) emission observed with JWST/MIRI provides a useful proxy for identifying supernova-driven bubbles. The statistics of these bubbles offer constraints on star formation and feedback models in galaxy simulations. Here, we combine PHANGS–JWST observations of NGC 628 with synthetic PAH images generated from FIRE-2 cosmological zoom-in simulations, post-processed using the radiative transfer code SKIRT with stochastic PAH emission. We introduce an automated bubble-finding algorithm to identify and characterize feedback-driven cavities in both datasets. The method performs well for prominent structures, though challenges remain for small-scale bubbles. Our bubble statistics reveal indications of molecular cloud fragmentation, motivating further refinement of the algorithm and application to a broader set of simulations and galaxies.

Key words: methods: numerical – galaxies: star formation – galaxies: ISM – ISM: bubbles

1 INTRODUCTION

Galaxy evolution is centered on star formation and stellar feedback (Tacconi et al. 2020). The interstellar medium (ISM) is substantially reshaped by the birth of large stars and their feedback through stellar winds, radiation pressure, and supernovae (SNe). These processes connect small-scale star formation to the large-scale structure and history of galaxies by controlling the rate of star formation, generating turbulence, enriching the ISM with metals, and driving galactic outflows. One outstanding issue facing contemporary astrophysics is understanding how star formation and subsequent feedback processes interact with and shape the evolution of the ISM.

Observationally, the evolution of the star-forming ISM across cosmic time is closely linked to feedback-regulated gas accretion and depletion (e.g. Tacconi et al. 2020). In particular, the observed relationship between the star formation rate and gas surface density was first established by Schmidt (1959) and later quantified by Kennicutt (1998), now commonly referred to as the Kennicutt–Schmidt (KS) relation. Semi-analytic models were the first to demonstrate that stellar feedback plays a critical role in self-regulating star formation within both molecular clouds and galactic discs (Faucher-Giguère et al. 2013). Therefore, the KS relation arises as a natural consequence of feedback-regulated star formation. More recently, high-resolution numerical simulations have provided more robust testbeds for reproducing and interpreting the observed Kennicutt–Schmidt relation (e.g. Faucher-Giguère 2018; Orr et al. 2018; Gurvich et al. 2020). However, these comparisons have focused on large physical scales ($\gtrsim$100 pc) due to the limited resolution of observations.

The James Webb Space Telescope (JWST) has opened a new window into this problem. With its unprecedented angular resolution and sensitivity in the mid-infrared, JWST enables detailed studies of stellar feedback-driven structures in nearby galaxies. In particular, the PHANGS–JWST survey (Lee et al. 2023) provides high-resolution photometric imaging of star-forming regions and feedback bubbles across a representative sample of spiral galaxies in mid-infrared, providing the astronomy community a new avenue for investigating the interplay of star formation and the ISM at physical scales of just a few parsecs. For insta, we can resolve the borders of supernova-driven bubbles in the PAH maps (Watkins et al. 2023) thanks to PHANGS–JWST's extraordinary resolution, which provides fresh information on the size and shape of feedback processes.

With the improvement of telescope, stellar feedback structures like superbubbles and shells, which are essential for forming the interstellar medium (ISM) and controlling galaxy growth, can be traced with dust emission rather than gas. JWST provides high-resolution imaging at 7.7 μm and 21 μm, where polycyclic aromatic hydrocarbons (PAHs) exhibit strong emission features. Although PAHs contribute less than 5% to the total dust mass, and dust represents only 1% of the ISM by mass, they are the most abundant dust species by number, are present in nearly all ISM phases of Milky Way–mass galaxies, and contribute a significant fraction (∼1/3) of the infrared luminosity. Their strong mid-infrared emission features, particularly the 7.7, μm band, make them easily detectable in observations and valuable tracers of galactic evolutionary processes and stellar feedback. However, PAHs are not a perfect tracer of gas since their small size makes them

★ E-mail: edn9cc@virginia.edu

fragile and vulnerable to destruction processes. Therefore, with gas distribution from simulation, it is essential to apply radiative transfer codes to directly compare simulations and observations.

Observations of PAHs in the HII regions around young, massive stars have found significant PAH destruction(Sutter et al. 2024; Chown et al. 2025). Expanding shock fronts driven by supernova feedback push gas and PAHs outward, creating cavities in the surrounding medium. Apart from this displacement, the characteristic bubble-like patterns seen in PAH emission maps are also left behind by the destruction of PAHs in supernova-driven shocks (Kirchschlager et al. 2022). Therefore, these PAH-deficient areas are indicators of recent massive star formation and the feedback activity that followed. However, PAHs are not a perfect tracer of gas since their small size makes them fragile and vulnerable to destruction processes. Therefore, with gas distribution from simulation, it is essential to apply radiative transfer codes to directly compare simulations and observations.

Direct comparisons between observations and simulations are essential but non-trivial. To compare these results, one must forward-model simulations into observable quantities. In this work, we use FIRE-2 cosmological zoom-in simulations Hopkins et al. (2018), which model star formation and feedback in a cosmological context, and post-process them with the Monte Carlo radiative transfer code SKIRT (Camps & Baes 2020) to produce synthetic JWST F770W photometric images of spiral galaxies. By treating simulations as observed, we can place them on equal footing with PHANGS–JWST data and directly test how stellar feedback manifests in both environments.

Supernova-driven bubbles serve as crucial tracers of stellar feedback, providing insight into how star formation shapes and regulates the surrounding interstellar medium (ISM). In their study of NGC628, (Watkins et al. 2023) manually identified feedback-driven bubble structures using JWST F770W, optical B-band, and Hα emission, and analyzed their size distribution, clustering properties, and morphological features. Building on this approach, we are trying to develop a systematic bubble-finding algorithm capable of automatically detecting and characterizing feedback-driven structures. Our method enables the robust measurement of bubble sizes, locations, separations, and spatial distributions, and can be applied uniformly to both observational data and galaxy-scale simulations, facilitating scalable and quantitative studies of stellar feedback across different environments. We may learn more about the timing, magnitude, and geographical effects of stellar feedback processes as well as how they influence galaxy evolution by examining their form and distribution. In this work, we use data from the PHANGS–JWST survey (Lee et al. 2023; Chown et al. 2025) to focus on the nearby spiral galaxy NGC 628. High-angular-resolution mid-infrared imaging of neighboring galaxies is provided by this survey; the spatial resolution for NGC 628 is about 12 pc. In particular, we examine data from the F770W filter, it tracks emissions around 7.7μm which is the brightest PAH features.

In this paper, we present our galaxy simulations and bubble finding algorithm in Section 2. We provide our results and discussion in Section 3. Lastly, we list our conclusions in Section 4.

2 METHODS

2.1 PHANGS-JWST Observations

The Physics at High Angular resolution in Nearby GalaxieS (PHANGS)–JWST survey mapped the infrared emission from young stellar populations and the dusty ISM across galaxy disks on scales of tens of parsecs with JWST acquired in Cycle 1 (ID 02107; PI: J. C. Lee). The observations use MIRI (F770W, F1000W, F1130W, and F2100W) and NIRCam (F200W, F300M, F335M, and F360M) imagery to target 19 nearby star-forming galaxies. For this work, we focus on MIRI F770W observations of NGC 628. The 7.7 μm PAH feature is the brightest feature and exhibits the best contrast in structure, and structure of NGC 628 has previously been studied by Watkins et al. (2023) The 1σ sensativity of these images is 0.11−0.15 MJy, and the spatial resolution is 12 pc (Lee et al. 2023).

2.2 Cosmological Galaxy Simulations

For our mock image creation and analysis, we utilize the cosmological zoom-in simulation **m12i**, presented in Hopkins et al. (2018), a MW-mass spiral galaxy at present day. This simulation is part of the Feedback In Realistic Environments (FIRE)[1] project, specifically the "FIRE-2" version of the code; all details of the methods are described in Hopkins et al. (2018), Section 2. The simulations use the code GIZMO (Hopkins & Raives 2016),[2], with hydrodynamics solved using the mesh-free Lagrangian Godunov "MFM" method. Both hydrodynamic and gravitational (force-softening) spatial resolution are set in a fully-adaptive Lagrangian manner; mass resolution is fixed. The simulations include cooling and heating from a meta-galactic background and local stellar sources from $T \sim 10 - 10^{10}$ K; and stellar feedback from OB & AGB mass-loss, SNe Ia & II, and multi-wavelength photo-heating and radiation pressure; with inputs taken directly from stellar evolution models. The FIRE physics, source code, and all numerical parameters are *exactly* identical to those in Hopkins et al. (2018). Since we are interested in constraining star formation criteria, we provide a brief summary of the criteria used in FIRE-2. Gas cells are converted to star particles if they are self-gravitating, Jean's unstable, a converging flow, molecular, and have $n_{\rm H} > 1000$ cm^3.

2.3 Creating Photometric Images

To model the impact of stellar feedback on dust emission, we generate synthetic JWST F770W observations using the SKIRT Monte Carlo radiative transfer code (Camps & Baes 2020), applied to snapshots from the FIRE-2 simulation. This approach allows us to generate synthetic JWST observations by accounting for absorption, scattering, and re-emission of starlight by dust, including stochastic heating of PAHs. In our setup, we use 10^{10} photon packages to apply Monte Carlo radiative transfer, we also make the convergence test to ensure the photon number we applied is reliable in Appendix A.

The radiative transfer is performed on a Voronoi spatial grid, with the Voronoi sites defined by the positions of gas particles in our simulation. Since our simulations do not track the evolution of dust directly, we adopt an assumed dust population (Narayanan et al. 2015; Ma et al. 2019; Choban et al. 2022). This approach enables a physically consistent modeling of absorption, scattering, and thermal re-emission processes within the dusty ISM. To model the mid-infrared PAH emission, we use the stochastic heating mode in SKIRT, following their size- and temperature-dependent emissivity model. We set the instrument to be face-on with the galactic disk with physical resolution of 12 pc, similar to PHANGs-JWST observation for NGC 628. The dust mass is assigned based on local gas mass,

[1] http://fire.northwestern.edu
[2] http://www.tapir.caltech.edu/~phopkins/Site/GIZMO.html

metallicity, and a dust-to-metal ratio (D/Z) prescription, assuming a **?** MW dust composition. To understand the sensitivity of our synthetic images to different dust prescription, we test (1) a constant $D/Z = 0.5$ prescription for all gas below $T < 10^6$ K to account for dust destruction via thermal sputtering and (2) a constant $D/Z = 0.5$ prescription for all gas below $T < 10^4$ K, and $D/Z = 0.1$ prescription for all gas between 10^4K and 10^6K to account for PAH destruction via photodestruction in HII regions.

We use the built in JWST F770W broadband transmission curve in SKIRT to illustrate the distribution of 7.7 μm PAH emission across the simulated galaxy. We also convolve the images with the F770W PSF taken from STSci PSF tool (Perrin et al. 2014) and inject noise via sampling from a Gaussian matching the 1-sigma detection threshold listed in the Lee et al. (2023). This forms the basis for our synthetic bubble analysis.

2.4 Bubble Identification

Our bubble-finding algorithm is based on the algorithm presented in Wallin et al. (2025), which was developed to examine the morphological characteristics of superbubbles in 21 cm radio emission maps. Intensity thresholding is the algorithm's fundamental idea: areas with surface brightness below a predetermined threshold are recognized as potential feedback bubbles. Our algorithm consists of the following steps:

Step 1: Starting with a JWST F770W surface brightness map, we embed the image in a square array, which corresponding to physical size in 10 kpc for both JWST and FIRE image.

Step 2: Within the disc map, we first calculate the surface brightness percentile for whole image, then we identify all regions that fall below a surface brightness threshold by each pixel, where the threshold is defined relative to the galactocentric distance.

Step 3: From these candidate regions, we apply morphological filtering to exclude structures that are unlikely to represent supernova-driven bubbles. For instance, the region close to the border of the image will be removed since it may not contain whole bubble. The remaining regions are then classified as bubble candidates for further analysis.

We extract the morphological data, such as radius, centroid position, and projected area, from the set of clearly defined bubble structures that are produced by this method. For the radius, we assume that each bubble is approximately circular and derive it from the total projected area. These measurements serve as the foundation for cross-comparisons between simulated and observed PAH maps, bubble size distribution calculations, and spatial clustering statistics.

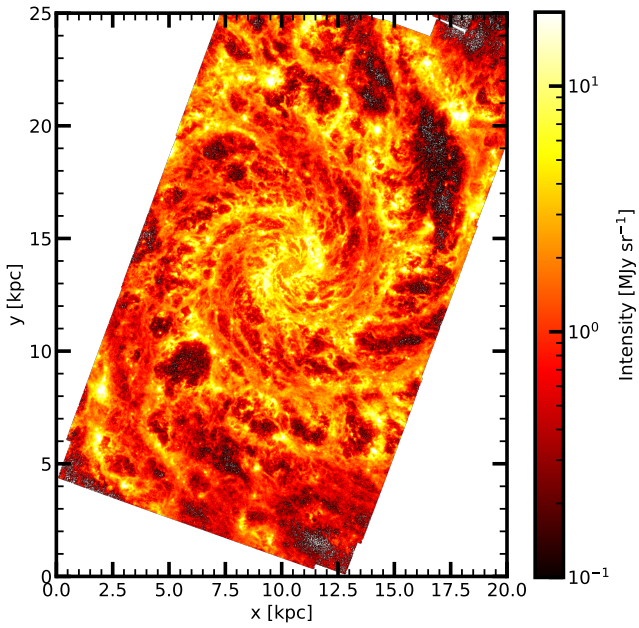

Figure 1. Mid infrared observation for nearby star-forming galaxy NGC 628 taken from Lee et al. (2023). We show the 7.7μm with F770W filter from MIRI JWST.

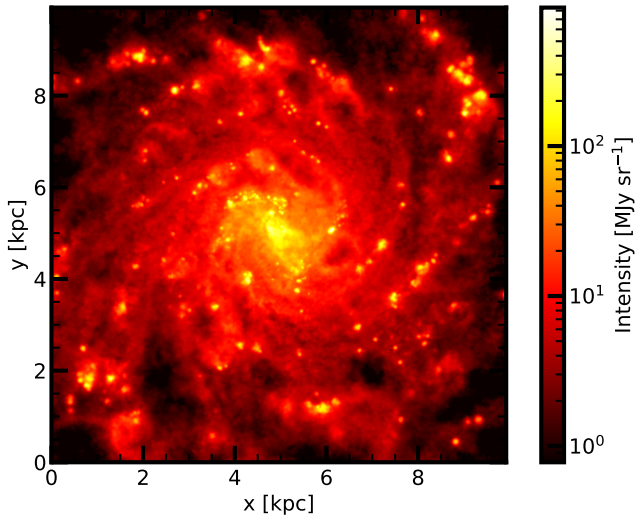

Figure 2. The 7.7μm map generated using SKIRT to apply radiative transfer to a star-forming galaxy simulation from FIRE-2.

3 RESULTS AND DISCUSSION

3.1 Qualitative First Look

The observed PAH emission map of NGC 628 from JWST and a synthetic PAH map produced from a FIRE-2 simulation with constant D/Z are directly compared in Figure 1 and 2. The generated map appears smoother and more diffuse, while the JWST map shows more distinct feedback structures, such as resolved bubble boundaries and filamentary features. On the other hand, FIRE image shows higher intensities, even with the matching resolution.

The higher overall intensities seen are due to the 4x higher SFR of m12i compared to NGC 628. Since PAHs are stochastically heated, any increase in the SFR, and thus the number of UV photons, will increase the PAH emission by a similar proportion (Draine & Li 2001). Moreover, in Figure 2, we see more PAH emission in bubbles since we do not account for PAH destruction.

Nevertheless, improved structural clarity is not always the result of this brightness increase. A more significant contributor may be the vertical thickness of the galactic disk. In our simulation, the gaseous disk is likely thicker than that of NGC 628. A thicker disk can obscure supernova-driven bubbles, especially in face-on projection, as overlapping layers of dust and PAH emission from the foreground and background fill in otherwise sharp cavities. The contrast of feedback-driven structures in PAH maps is improved by thinner disks, which more easily display distinct cavities and shells. The significance of

disk geometry in interpreting PAH-based tracers of star feedback is highlighted by this morphological dependence and tests with FIRE galaxies with thin disc morphologies will be necessary to understand its effects.

In Figure 3, we show the results of our bubble-finding algorithm applied to both the JWST F770W PAH map of NGC 628 and the synthetic PAH map generated from the FIRE-2 simulation. We assume all bubbles are circular, with the bubble radius calculated from the bubble area identified by our algorithm. Each cyan circle marks a bubble identified by the algorithm. The technique works well overall, identifying a large number of the observable bubble formations in both datasets. Since the JWST data has more clear PAH features, it is reasonable that the algorithm detects more bubbles in NGC 628. The smoother emission from the FIRE simulation can mask small-scale cavities and result in fewer total number of bubbles detected, especially small bubbles, in the FIRE image.

There are still certain restrictions, though. Regions that are visually compatible with bubble morphology but were missed by the algorithm. For instance, the smaller structures near the galactic center of FIRE image and the structures between two spiral arms in JWST image. These false negatives are excluded under the existing detection criteria because they usually occur in areas where the bubble boundaries are not well defined by surface brightness thresholds. A planned future development is to increase the algorithm's sensitivity to such ambiguous structures, perhaps using machine learning classifiers or adaptive thresholding.

3.2 Bubble Statistics

We next examine the bubble size distributions for both NGC 628 and the FIRE simulation, shown in Figure 4. The distributions are well described by power-law fits, with NGC 628 exhibiting a steeper slope (i.e., higher power-law index) than the FIRE galaxy. This suggests that NGC 628 contains a higher proportion of small bubbles, consistent with its sharper, better-resolved PAH features. The FIRE galaxy, by contrast, displays a shallower slope, indicating fewer small cavities. This may again be attributed to the increased vertical thickness of the simulated disk, which tends to blur or obscure compact feedback structures in projection.

Finally, we compute the two-point correlation function (2PCF) for the detected bubble populations in both datasets. This statistical tool quantifies the excess probability (relative to random) of finding bubble pairs at a given projected separation. The two-point correlation function of bubbles provides a statistical measure of how clustered feedback structures are, which in turn reflects the underlying spatial distribution of star formation and the efficiency of stellar feedback in shaping the interstellar medium.

The results, shown in Figure 5, reveal that small bubbles exhibit stronger clustering on sub-kiloparsec scales compared to larger ones. One possible interpretation is that molecular clouds fragment and collapse into stellar populations, our result might be an indication of the fragmentation of massive molecular clouds. As molecular clouds fragment and collapse into multiple nearby stellar populations, their subsequent feedback produces spatially correlated bubble structures. In consequence, comparing 2PCF could provide constraints on star formation. This scenario encourages more research into the spatial relationship between stellar age, bubble location, and ISM morphology. In addition, comparisons with galaxy simulations employing different star formation prescriptions will be necessary to assess whether bubble clustering statistics can serve as a constraint of star formation models.

Even though these preliminary results offer insightful information, more comparisons over a larger sample of observed and simulated galaxies and continuous improvement of the bubble recognition system are necessary to validate and generalize these tendencies.

4 CONCLUSIONS AND FUTURE WORKS

In this work, we generated mock JWST–MIRI F770W images of a FIRE-2 galaxy using the Monte Carlo radiative transfer code SKIRT, including a treatment for stochastic PAH emission. We then adapted a bubble-finding algorithm from Wallin et al. (2025) to identify supernova-driven bubbles in both the synthetic images and PHANGS–JWST observations of NGC 628. By applying this method to simulated and observed data, we compared the statistical properties of bubble populations and separation across the two images.

This work highlights several key findings and directions for continued research, the PHANGS–JWST survey offers a powerful tool for probing the star formation history of galaxies through high-resolution PAH emission maps. We provide a bubble finding algorithm and apply bubble statistics analysis on both observation and simulation to investigate stellar feedback during galaxy evolution. The bubble size distribution showed that NGC 628 contains a larger number of supernova-driven bubbles, particularly at small sizes. This comparison suggests that the vertical thickness of a galaxy's disk can significantly influence the visibility and morphology of PAH structures, including SNe-driven bubbles. Furthermore, the two-point correlation function reveals that small-scale bubbles tend to be more strongly clustered in both the simulated and observed maps. We propose a working hypothesis in which fragmentation of giant molecular clouds leads to the formation of spatially clustered star-forming regions, naturally resulting in the observed clustering of feedback bubbles.

Looking ahead, we plan to refine and expand our bubble-finding algorithm to enable a unified and scalable methodology for researching stellar feedback mechanisms across both simulated images from simulation and PHANGS-JWST images beyond NGC 628. We will also test our assumptions using additional simulation suites, such as FIRE-3 and Auriga, and extend the analysis to a broader sample of galaxies. In parallel, we are exploring more complex prescriptions for PAH destruction, particularly temperature-dependent models, to capture the dependence of PAH abundance with environment. Incorporating these improvement in PAH modeling and test different star formation and feedback treatments will enable tighter constraints on the connection between stellar feedback, ISM structure, and galaxy evolution.

ACKNOWLEDGEMENTS

This work originated from a project of the Summer Program in Astrophysics 2025 held at the University of Virginia, and funded by the Center for Global Inquiry and Innovation, the National Science Foundation (Grant 2452494), the National Radio Astronomy Observatory (NRAO), the Kavli Foundation and the Heising-Simons Foundation.

DATA AVAILABILITY

The inclusion of a Data Availability Statement is a requirement for articles published in MNRAS. Data Availability Statements provide a standardised format for readers to understand the availability of data underlying the research results described in the article. The statement may refer to original data generated in the course of the study or to

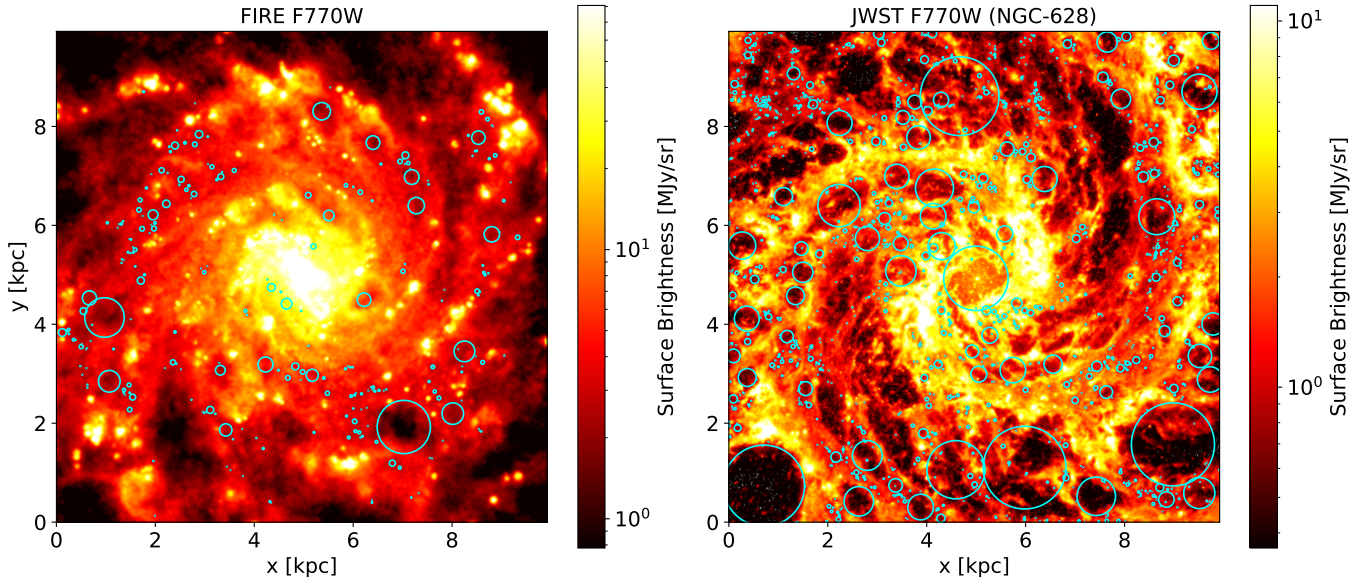

Figure 3. Bubble location identified in MIRI F770W JWST data for NGC 628 (left) and FIRE simulation (right) with our modified bubble finding algorithm from Wallin et al. (2025), cyan circles represent the location and size of each bubble.

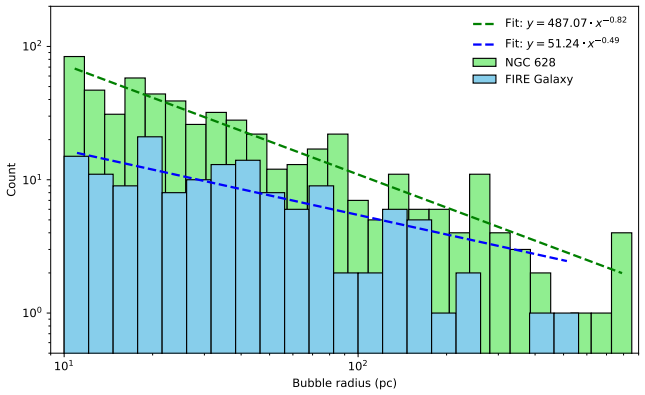

Figure 4. Size distribution of bubbles for FIRE simulation (upper) and NGC628 from JWST(lower), dashed red line is the power-law fit to the distribution equal to p = -0.54 and -1.05 respectively.

third-party data analysed in the article. The statement should describe and provide means of access, where possible, by linking to the data or providing the required accession numbers for the relevant databases or DOIs.

REFERENCES

Camps P., Baes M., 2020, Astronomy and Computing, 31, 100381
Choban C. R., Kereš D., Hopkins P. F., Sandstrom K. M., Hayward C. C., Faucher-Giguère C.-A., 2022, MNRAS, 514, 4506
Chown R., et al., 2025, A&A, 698, A86
Draine B. T., Li A., 2001, ApJ, 551, 807
Faucher-Giguère C.-A., 2018, MNRAS, 473, 3717
Faucher-Giguère C.-A., Quataert E., Hopkins P. F., 2013, MNRAS, 433, 1970
Gurvich A. B., et al., 2020, MNRAS, 498, 3664
Hopkins P. F., Raives M. J., 2016, MNRAS, 455, 51
Hopkins P. F., et al., 2018, MNRAS, 480, 800
Kennicutt Jr. R. C., 1998, ApJ, 498, 541
Kirchschlager F., Mattsson L., Gent F. A., 2022, MNRAS, 509, 3218
Lee J. C., et al., 2023, ApJ, 944, L17
Ma X., et al., 2019, MNRAS, 487, 1844
Narayanan D., et al., 2015, Nature, 525, 496
Orr M. E., et al., 2018, MNRAS, 478, 3653
Perrin M. D., Sivaramakrishnan A., Lajoie C.-P., Elliott E., Pueyo L., Ravindranath S., Albert L., 2014, in Oschmann Jr. J. M., Clampin M., Fazio G. G., MacEwen H. A., eds, Society of Photo-Optical Instrumentation Engineers (SPIE) Conference Series Vol. 9143, Space Telescopes and Instrumentation 2014: Optical, Infrared, and Millimeter Wave. p. 91433X, doi:10.1117/12.2056689
Schmidt M., 1959, ApJ, 129, 243
Sutter J., et al., 2024, ApJ, 971, 178
Tacconi L. J., Genzel R., Sternberg A., 2020, ARA&A, 58, 157
Wallin B., Wibking B. D., Voit G. M., 2025, MNRAS, 538, 2427
Watkins E. J., et al., 2023, ApJ, 944, L24

APPENDIX A: CONVERGENCE TEST

We conduct a series of experiments with different numbers of photon packets to evaluate the numerical convergence and robustness of our radiative transfer results. Increasing photon counts reduces statistical noise, as seen in Figure A1 (left), with brightness variations across most locations limited to 10%. Furthermore, we calculate the per-pixel relative error (Figure A1, right), which measures the degree of uncertainty in the model output; green pixels stay within acceptable noise limits, while yellow pixels show very convergent regions. These diagnostics collectively verify that our SKIRT simulations are numerically stable and appropriate for quantitative examination of feedback structures and PAH morphology.

This paper has been typeset from a TEX/LATEX file prepared by the author.

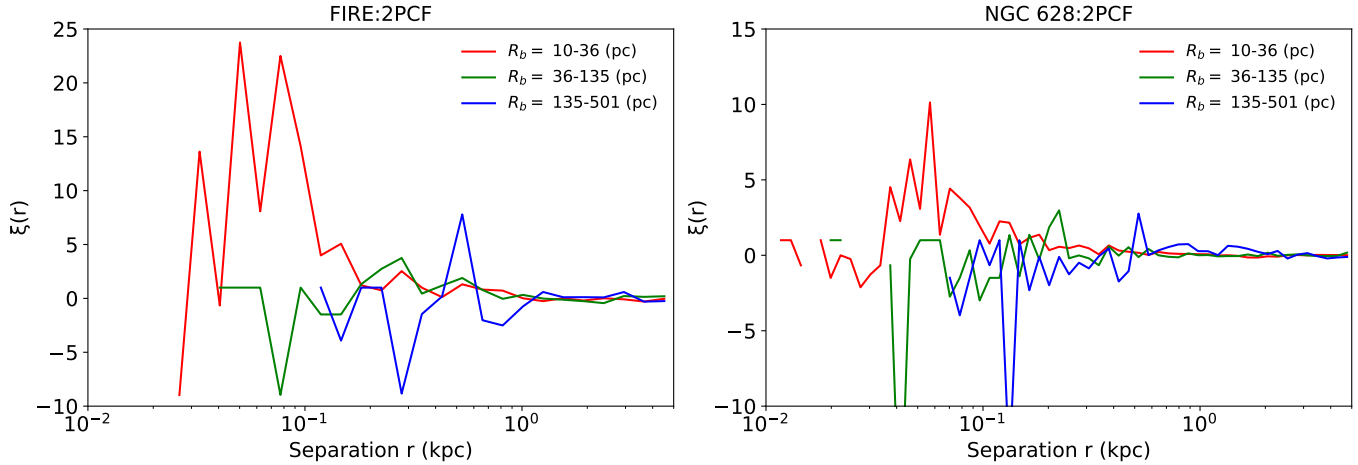

Figure 5. Two point correlation function for FIRE image(left) and NGC628(right). The red lines represent the small scale bubbles; the green lines show the medium size bubbles; and the blue lines indicate the large bubbles.

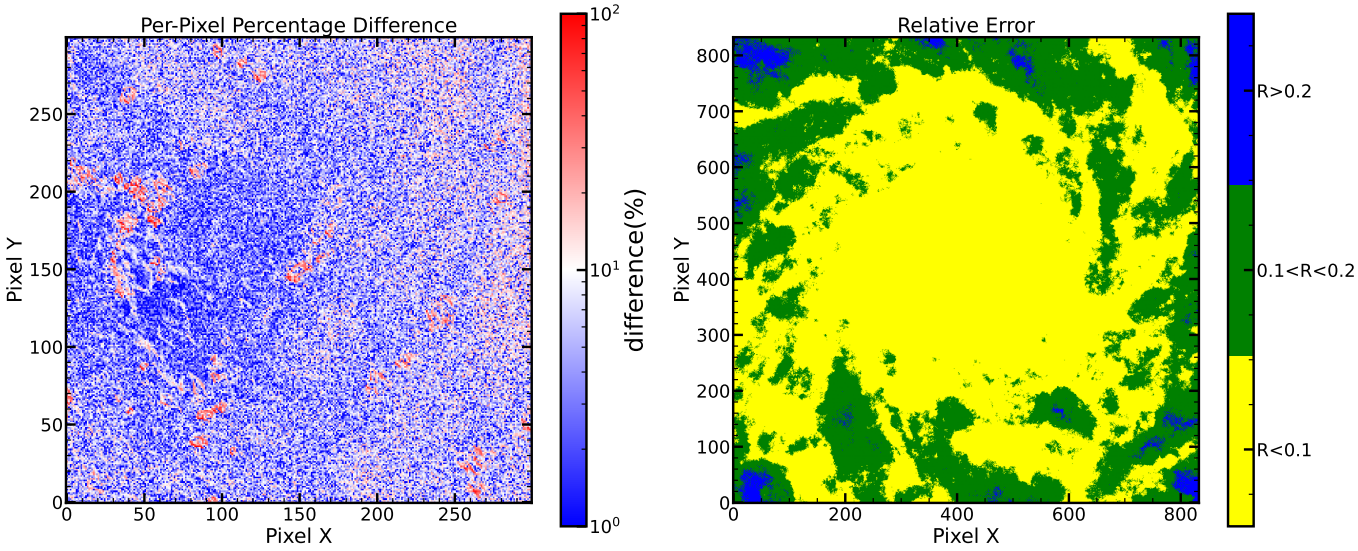

Figure A1. Convergent test with different photon number in FIRE simulation, 10^{10} photon... The reliability statistics for simulated fluxes, most of region with relative error less than 0.1 which providing high confidence of our result.